Monthly Notices
of the
ROYAL ASTRONOMICAL SOCIETY

MNRAS **496,** 903–912 (2020)
Advance Access publication 2020 June 9

doi:10.1093/mnras/staa1593

A search for γ-ray emission from a sample of local Universe low-frequency selected radio galaxies

Max Harvey ,★ Cameron B. Rulten and Paula M. Chadwick

Centre for Advanced Instrumentation, Department of Physics, University of Durham, South Road, Durham DH1 3LE, UK

Accepted 2020 June 1. Received 2020 June 1; in original form 2019 December 19

ABSTRACT

Radio galaxies are uncommon γ-ray emitters, and only low-redshift radio galaxies are detected with the *Fermi* Large Area Telescope (*Fermi*-LAT). However, they offer potential insights into the emission mechanisms of active galaxies, particularly as the alignment of their jets with respect to the Earth means that, unlike blazars, their emission is not necessarily jet dominated. We use the *Fermi*-LAT data to perform an unbiased survey of 78 radio galaxies from the Bologna complete sample in order to search for new γ-ray-emitting radio galaxies. We observe statistically significant γ-ray emission from four of the six known *Fermi*-LAT-detected radio galaxies included in this sample, and find some evidence for γ-ray emission spatially coincident with four previously undetected radio galaxies. As a large parameter space is searched, we calculate a probability distribution to compute the look-elsewhere effect. We find that these four spatially coincident sub-threshold γ-ray excesses are most likely a chance association, and are unlikely to be emission from the radio galaxies. Upper limits on flux are calculated for the radio galaxies from which no γ-ray emission is observed.

Key words: methods: statistical – galaxies: active – galaxies: jets – gamma-rays: galaxies.

1 INTRODUCTION

1.1 Radio galaxies

Active galactic nuclei (AGNs) can be divided into two broad classes: radio-quiet AGNs, which have little to no radio emission relative to other wavebands, and radio-loud AGNs, which have dominant radio emission relative to other wavebands. It is the radio-loud AGNs, primarily blazars and radio galaxies, that are the most prominent in the γ-ray sky. Both have powerful radio jets, up to kiloparsec (kpc) scales in many cases, and are considered to be fundamentally the same objects viewed at different orientation angles.

Blazars are radio-loud AGNs that are viewed nearly directly down the jet, from which we see variable and luminous radio emission dominated by Doppler boosting of the electromagnetic radiation in the jet. In the γ-ray sky, over 90 per cent of extragalactic objects detected are blazars, i.e. BL Lacs and flat-spectrum radio quasars (FSRQs; Massaro, Thompson & Ferrara 2016; Abdollahi et al. 2020). There is a general consensus that the γ-rays are produced through inverse Compton scattering by electrons in the jet, but other mechanisms are possible (e.g. Boettcher et al. 2013). However, most AGNs are not viewed from such a small angle; the bulk of the radio-loud population, the radio galaxies (Urry & Padovani 1995; Atwood et al. 2009), is viewed from a larger orientation angle relative to the jet, so that the observed emission is not necessarily dominated by Doppler boosting in the jet.

The larger orientation angles of radio galaxies allow us to view their extended structure; thus, we are able to define some differences between two types of kpc-scale jet: Fanaroff–Riley I (FR I) radio galaxies have 'low-power' sub-relativistic kpc-scale jets, which are radiatively inefficient, edge darkened, and terminate in radio plumes. On the other hand, Fanaroff–Riley II (FR II) radio galaxies have 'high-power' mildly relativistic kpc-scale jets, are more radiatively efficient than FR I galaxies, and are edge brightened, terminating in radio lobes containing hotspots of radio emission (Fanaroff & Riley 1974). On a parsec scale, close to the radio core, the jets of FR I and FR II radio galaxies are identical (Giovannini et al. 1994). It is thought that FR I radio galaxies are the parent population of the BL Lac blazar class, and FR IIs are the parent population of FSRQs (Urry & Padovani 1995;Grandi & Torresi 2012).

1.2 γ-ray observations

Launched in 2008, the *Fermi* Large Area Telescope (*Fermi*-LAT) has been observing the whole sky over an effective γ-ray energy range of 100 MeV to approximately 300 GeV for over a decade. Varying levels of γ-ray emission have been detected in both FR I and FR II radio galaxies (Abdo et al. 2009; Rulten, Brown & Chadwick 2020). There is evidence for γ-ray production in both the radio core of the galaxy, from the parsec-scale jet (Angioni et al. 2019), and

★ E-mail: max.harvey@durham.ac.uk

the kpc-scale jets for both galaxy types (Abdo et al. 2010; Grandi & Torresi 2012).

There is also evidence for γ-ray emission from a third type of radio galaxy, the FR 0, or 'compact' radio galaxy (Baldi & Capetti 2009; Baldi, Capetti & Giovannini 2016). A relatively recent addition to the FR classification system, the FR 0 radio galaxy is defined by a core to total emission ratio 30 times that of the FR I, and is believed to be an early evolutionary phase in the activity of an FR I radio galaxy that is lacking extended radio emission in kpc jets (Garofalo & Singh 2019). Despite the FR 0 class being the most numerous type of radio galaxy in the local Universe, almost all of the radio galaxies with detected γ-ray emission are FR I or FR II in nature.

1.3 Spectral features in AGNs and the Bologna complete sample

The Bologna complete sample (BCS; Giovannini et al. 2005; Liuzzo et al. 2009) is a catalogue of 95 radio-loud AGNs. The BCS contains two BL Lac blazars, Mrk 421 and Mrk 501, and 93 radio galaxies of varying kpc-scale jet morphology. Of the 95 galaxies in the complete catalogue, 8 are included in the fourth *Fermi* Point Source Catalogue (4FGL; Abdollahi et al. 2020): Mrk 421 and Mrk 501, the FR I galaxies NGC 315, NGC 2484, 3C 264, and 3C 274 (M 87/Virgo A), 4C 29.41, and the FR 0 galaxy 4C 39.12.

The BCS is a particularly interesting sample for investigating the characteristics of γ-ray emission from radio galaxies. It is drawn from the 3CR (Bennett 1962) catalogue (178 MHz) and B2 catalogue (408 MHz; Colla et al. 1970, 1972, 1973; Fanti et al. 1974). The authors impose no selection criteria on core radio power, orientation angle, or the velocity of the jet. The primary selection criteria are a redshift limit ($z < 0.1$), and a cut on Galactic latitude, keeping only sources where $|b| > 10^{\circ}$. The precursor to the BCS, the Bologna strong core sample (BSCS; Giovannini, Feretti & Comoretto 1990, and following works), had a core flux limit, which meant that the BSCS was inherently biased towards more Doppler-boosted sources with smaller orientation angles and therefore dominated by emission from the kpc-scale jet. The BCS, however, has no such limit, and consequently has a range of sources with a variety of orientations.

Most detected γ-ray-emitting radio galaxies are low-redshift objects ($z < 0.1$); therefore, we expect that any new radio galaxy detections with *Fermi*-LAT would have similarly low redshifts. In order to check that the *Fermi*-LAT-detected radio galaxies and the BCS have similar redshift distributions, we employ a two-sample Kolmogorov–Smirnov (KS) test[1] between the 4FGL γ-ray-emitting radio galaxies and the BCS radio galaxies. We find a p-value of 0.131, indicating reasonable similarity between the 4FGL radio galaxies' redshifts and those of the BCS objects (Table A1).

There is also a connection between the flux levels of the radio and optical wavebands in radio galaxies (Owen & Ledlow 1994). A two-sample KS test comparing the observed absolute magnitudes of the BCS radio galaxies with those of the *Fermi*-LAT-detected radio galaxies gives a p-value of 0.949, indicating that the optical luminosity distribution of the radio galaxies in the BCS is similar to that of the γ-ray radio galaxies.

The closest AGN to the Earth, the FR I radio galaxy Centaurus A (Cen A), shows an unusual spectral feature in γ-rays. Due to its proximity, Cen A is one of two radio galaxies where significantly extended γ-ray emission is seen with *Fermi*-LAT (Abdo et al. 2010), the other being Fornax A (Ackermann et al. 2016). In Cen A, the *Fermi*-LAT data show a distinct γ-ray core and lobe structure consistent with the positions of the radio core and lobes. Brown et al. (2017) analysed the core emission, and found a statistically significant (5σ) hardening in the *Fermi*-LAT spectrum, with a break energy of 2.6 ± 0.3 GeV. This spectral feature is compatible with a 'spike' in the dark matter halo profile, but could also be produced by a population of unresolved millisecond pulsars or signatures of cosmic ray acceleration. All of these hypotheses are consistent with γ-ray emission that does not originate in the kpc-scale jet. Recent observations with the H.E.S.S. γ-ray telescope facility suggest that the highest energy emission may in fact come from an inner parsec-scale jet, close to Cen A's core (Sanchez 2018). This result is consistent with the results of Angioni et al. (2019), where they find that pc-scale jets drive the γ-ray emission in galaxies that are not dominated by Doppler-boosted emission.

Rulten et al. (2020) examined 26 *Fermi*-LAT-detected radio galaxies for Cen A-like spectral features, but found no evidence of spectral hardening in the 10 yr average spectra among the radio galaxies that showed no evidence for variability. In this work, we search for γ-ray emission from a sample of close, low-frequency radio galaxies that are unlikely to be dominated by Doppler-boosted γ-ray emission (blazar-like emission). This would constitute evidence for large-scale emission processes that are not associated with a jet occurring in these objects.

In Section 2, we discuss the selection of the BCS galaxies discussed in this paper, and in Section 3 we describe our analysis of the *Fermi*-LAT data. Our results are given in Section 4, and our statistical analysis is provided in Section 5. Finally, some discussion and conclusions are given in Sections 6 and 7, respectively.

2 SELECTION CRITERIA

Not all of the 95 galaxies in the 2005 edition of the BCS (Giovannini et al. 2005) are suitable for our search with *Fermi*-LAT. The two Markarian objects are immediately discarded as they are blazars, and thus not relevant to our work. We discard any radio galaxy in the BCS without a clear 'FR I', 'FR II', or 'C' (FR 0) morphology since it would be difficult to draw any conclusions about such objects. The BCS authors' cuts on Galactic latitude and redshift are sufficient for our purposes, so we do not impose any further cuts. We also do not impose any cuts on radio luminosity, core radio power, or any other property at any wavelength.

We use the six objects with known γ-ray emission, which are included in the 4FGL, as a reference for the analysis of any newly detected sources rather than considering them within our search. Finally, several sources were discarded after initial analysis of the *Fermi*-LAT data, as the modelling close to the position of the target radio galaxy was of poor quality (for instance, due to very bright sources in the field of view). After applying our selection criteria, we are left with 72 target radio galaxies from which we attempt to find evidence of γ-ray emission, plus the 6 known 4FGL radio galaxies for reference. A full list of the galaxies included in the sample (including those with known γ-ray emission), with their morphology, coordinates, and redshift, is shown in Table A1.

For the purposes of this paper, we will refer to the target radio galaxies in our sample as TRGs, and those where a level of γ-ray emission is observed that is below the 5σ threshold for detection as sub-threshold γ-ray target radio galaxies (STRGs).

[1]The equation for the two-sample KS test is given as $D_{a,\,b} = \sup |F_{1,\,a(x)} - F_{2,\,b(x)}|$ for two samples $a(x)$ and $b(x)$, where $D_{a,\,b}$ is the KS statistic.

Table 1. The parameters used in the likelihood analysis of the square ROI around each TRG.

Observation period (dates)	04/08/2008–10/01/2020
Observation period (MET)	239 557 417–600 307 205
Observation period (MJD)	54682–58858
Energy range (GeV)	0.1–300
Data ROI width	20°
Model ROI width	30°
Zenith cut	<90°
Instrument response	P8R3_SOURCE_V2
Point source catalogue	4FGL
Isotropic diffuse	iso_P8R3_SOURCE_V2_v01
Galactic diffuse	gll_iem_v07

3 *FERMI*-LAT OBSERVATIONS AND ANALYSIS

The *Fermi*-LAT (Atwood et al. 2009) is a pair conversion telescope that detects the charged particles produced by γ-rays interacting with the detector, from which it is possible to reconstruct the energy, time of arrival, and incident direction of the photon. We take all-sky observations over an 11.5 yr period to execute our survey, with the parameters used in our observations and modelling shown in Table 1. The 11.5 yr period is chosen to maximize observation time, and runs from the beginning of the *Fermi*-LAT mission until the week when we began our analysis in 2020 January.

We use the Pass 8 *Fermi*-LAT data, which has improved analysis methods and event reconstruction over prior data sets. Using the parameters in Table 1, we execute a standard reduction chain using the *Fermi* Science Tools: energy cuts on photons, computing instrument live-time, etc. For each TRG, we consider a square region of interest (ROI) of 20° width around it, and bin all photons into spatial bins of 0.1° width in RA and Dec, and in 10 bins per decade for energy. We follow the well-established binned likelihood analysis method of Mattox et al. (1996), whereby maximum likelihood estimation is used to fit a model to our data set on a bin-by-bin basis. We use the 4FGL catalogue and background model components described in Table 1, to make predictions for the number of photons in each bin. To improve the accuracy of the predictions in the model, we first iteratively push the parameters close to the maximum likely values for each catalogued source in the model. We then free the spectral normalization of all sources in each ROI within 3° of the central, target radio galaxy, and free the normalization of both the isotropic and Galactic background components. We then perform a full maximum likelihood fit on the sources with freed normalization. To check our modelling, we compute a residual map, the difference between the observed and predicted counts on a bin-by-bin basis. Our residual map of the ROIs is shown in Fig. B2.

The majority of known γ-ray-emitting radio galaxies are point sources when viewed with *Fermi*-LAT. The test statistic (TS), used to measure source significance, is defined as the ratio between the likelihood of an alternative (Θ_1) and a null hypothesis (Θ_2), given by

$$\mathrm{TS} = 2 \ln \frac{L(\Theta_1)}{L(\Theta_2)}. \quad (1)$$

The null hypothesis is that there is no point source, and the alternative hypothesis is that there is one. Via Wilks' theorem (Wilks 1938), the TS corresponds to a value of χ^2 for k degrees of freedom.

We execute our survey by running the 'find sources' algorithm, included in the FERMIPY PYTHON module (Wood et al. 2017). This fits a test source at each point in our model, and calculates the TS of each of these. Where the TS corresponds to a significance of 3σ or greater, we add this permanently to our model. For a TS < 25, we have 3 degrees of freedom (RA, dec, and spectral normalization) because the algorithm iterates over RA and dec in order to find new sources not included in the 4FGL. For TS > 25, we have 4 degrees of freedom, as we fit spectral shape too. Our full sky TS map is shown in Fig. B1.

For a detection, we require a source significance greater than 5σ. Sources added to the model with significance $3 < \sigma < 5$, are not considered to be significantly detected γ-ray sources. Instead, we consider these to be 'sub-threshold' emission radio galaxies (STRGs), where there is a possibility of γ-ray emission, but the statistical significance is marginal.

Radio galaxies are generally variable on time-scales of months (Kataoka et al. 2010). NGC 1275 is one exception, with variability time-scales of hours, but it is a very luminous γ-ray source (Tanada et al. 2018). Another example would be the rapidly variable 3C 120, one of the more blazar-like objects in the γ-ray-emitting radio galaxy population (Janiak, Sikora & Moderski 2016). The majority of the population is less luminous in γ-rays, rendering flux variability on daily time-scales undetectable with current instrument sensitivity. None the less, it is possible that the radio galaxies in our sample might be detectable over a short time-scale (e.g. a month) but not when averaged over our observation time. Thus, we produce a light curve at the position of each radio galaxy, using monthly binning. We then calculate a TS for variability, and use this to see whether any of our sample is variable.

Should we detect a source with a significance over 5σ, the next step would be to compute a spectral energy distribution (SED) and then attempt to model any spectral features.

4 RESULTS

Sub-threshold (below 5σ) γ-ray excesses are found spatially coincident with 4 of the 72 radio galaxies in our sample, giving us four STRGs: B2 0800+24, B2 1040+31, 3C 293, and 3C 272.1. Of these, only one has TS > 25, the typical TS threshold used for a source to be catalogued in the 4FGL (Abdollahi et al. 2020). This radio galaxy is B2 0800+24, and it is discussed further in Section 4.1. For comparison, the six BCS radio galaxies that are known γ-ray emitters (in the 4FGL) were also modelled over an 11.5 yr period. Four of these had a significance of above 5σ, the exceptions being NGC 2484 and 4C 29.41. While these two 4FGL radio galaxies have previously been significant enough to be included in the *Fermi*-LAT point source catalogues, over an 11.5 yr observation time their TS has decreased, when compared to a shorter observation period. The results for all 10 galaxies are displayed in Table 2.

The light curves provide no evidence for significant γ-ray flaring or variability in our TRGs. For each light curve, a TS for temporal variability is calculated that corresponds to a χ^2 value. For STRGs, $\chi^2_{\mathrm{reduced}} > 1$ in all cases for the null hypothesis that there is no γ-ray variability. This indicates that the best model to fit the data is one with no variability in time. For TRGs with no γ-ray emission, $\chi^2_{\mathrm{reduced}} < 1$, which indicates that there are insufficient data to fit the model, therefore no evidence for variability.

As the four STRGs are all low in significance, it is not possible to perform any spectral analysis, and we interpret these results as 95 per cent upper confidence limits, which are calculated on the basis of an $E^2 \times$ differential flux. For the case of the 68 non-detections, upper limits are also calculated at the radio galaxies' positions. These upper limits are shown in Table A1.

Table 2. The 10 radio galaxies in our sample that show evidence for γ-ray emission. Most of the galaxies previously detected in the 4FGL are robustly detected in this analysis. The significance values quoted here are calculated using the given number of degrees of freedom for each 4FGL radio galaxy or STRG. The Fanaroff–Riley galaxy morphologies are taken from Giovannini et al. (2005), where those described as 'compact' radio galaxies in that paper are described as FR 0 radio galaxies here.

Galaxy	Morphology	4FGL?	TS
B2 1040+31	FR 0	No	20.47 (3.64σ)
3C 272.1	FR I	No	18.97 (3.45σ)
3C 293	FR I	No	20.33 (3.62σ)
B2 0800+24	FR I	No	28.47 (4.26σ)
4C 39.12	FR 0	Yes	86.19 (>5σ)
4C 29.41	FR I	Yes	20.85 (3.7σ)
NGC 315	FR I	Yes	106.3 (>5σ)
NGC 2484	FR I	Yes	26.63 (4.07σ)
3C 274 (M 87)	FR I	Yes	1813 ($\gg$5σ)
3C 264	FR I	Yes	165.8 (>5σ)

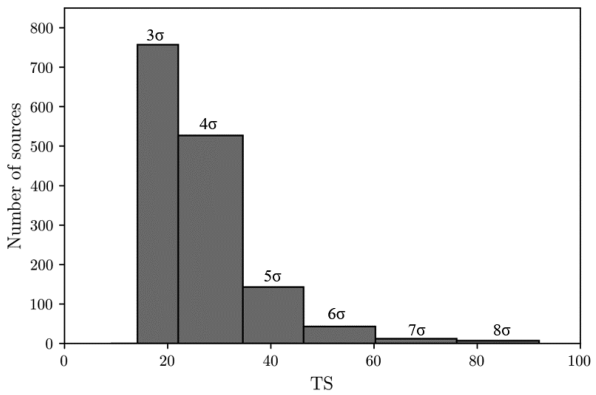

Figure 1. A histogram showing the TS values of all of the non-catalogued point sources modelled across all of the 78 ROIs. From left to right, the bins show the number of sources of 3σ, 4σ, 5σ, 6σ, 7σ, and 8σ significance, for the appropriate degrees of freedom in our likelihood analysis. We use the 3σ and 4σ sources (the two leftmost bins in this distribution) for our look-elsewhere effect calculation, as these represent the significances of the STRGs.

4.1 The marginal detection of B2 0800+24

Of the four STRGs, the only one that could be considered a possible detection is B2 0800+24, with a TS of 28.47. With 4 statistical degrees of freedom between the hypothesis of there being a γ-ray point source and the null hypothesis that there is not, this gives a 4.26σ significance, which meets the criterion for inclusion into the 4FGL (Abdollahi et al. 2020). In our survey, we regard 5σ as the threshold for detection, primarily because of the large population of <5σ sources, shown in Fig. 1. Our calculations in Section 5.1 demonstrate that sources below 5σ are likely to be caused by fluctuations in the γ-ray background.

5 STATISTICAL ANALYSIS

5.1 The look-elsewhere effect

We find four STRGs that may provide evidence for emission. However, we must ask the question, what is the probability that this γ-ray excess is just a fluctuation in the background that happens to resemble faint γ-ray emission from an STRG due to its position in the sky? This is the look-elsewhere effect, which is a phenomenon whereby a false positive result may arise as a direct result of searching a very large parameter space (Lyons 2008). Given we are searching in 72 places in the sky, we must quantify the look-elsewhere effect in order to work out the probability that our STRG observations are a false positive.

Our criterion for spatial coincidence was that the 99 per cent positional uncertainty ($r_{99\ \mathrm{per\ cent}}$) must be larger than the angular offset of the centre of the γ-ray emission from the TRG. Thus, it is possible to calculate the area of the sky covered by all of our detected point source positional uncertainties (A_{PS}). This is given by equation (2):

$$A_{\mathrm{PS}} = \sum \pi r^2_{99\,\mathrm{per\,cent}}. \tag{2}$$

Dividing this area by the total area analysed (A_{tot}), and accounting for overlaps between ROIs, gives us the probability of there being a point source of at least 3σ significance at any point in the sky (we will call this event x), i.e.

$$P(x) = \frac{A_{\mathrm{PS}}}{A_{\mathrm{tot}}}. \tag{3}$$

For our population of point sources across the whole area we have analysed, we find $P(x) = 0.027$. Using this probability, we can now calculate the probability that 4 STRGs are found, given we looked in 72 places. To do this, we look at the distribution of point sources across the sky, and select all of those with $3\sigma < \sigma_{\mathrm{PS}} < 5\sigma$, where σ_{PS} is the point source significance. The TS distribution of all point sources across all our ROIs is shown in Fig. 1.

Using the distribution shown in Fig. 1, we combine the 3σ and 4σ bins and look at the spatial distribution of these point sources. Employing our false positive probability, $P(x) = 0.027$ (which was calculated for $3\sigma < \sigma_{\mathrm{PS}} < 5\sigma$ point sources), we set $P(x) = p$ for convenience. We then define our total number of search points in the sky, $N = 72$ and assume that these are distributed randomly across our total analysed area. We also assume that there is no underlying pattern in the spatial distribution of the point sources; as we are looking solely at the extragalactic sky, this is a valid assumption to make. Next we define a new variable, y, that represents the number of point sources in our TS range that are spatially coincident with our TRGs. For our results, $y = 4$. However, by varying y from $0 \rightarrow 72$, we are able to calculate a full probability distribution for the number of chance spatial correlations between TRGs and $3\sigma < \sigma_{\mathrm{PS}} < 5\sigma$ point sources on the basis of the probability mass function for the binomial distribution,[2] as we are effectively modelling the success rate of sampling with replacement, given in equation (4):

$$P(y) = \binom{N}{y} p^y (1-p)^{(N-y)}. \tag{4}$$

This probability distribution is shown in Fig. 2, and we see that the probability of obtaining four STRGs through chance spatial correlation is 8 per cent, with the chance of at least one STRG being a false positive being 75 per cent.

[2]Although we do not actually replace our sources, with approximately 2000 point sources in our model, the value of $P(x)$ does not significantly change with each association. If we had a number of successful spatial associations that was comparable with our overall sample size, the probability mass function for the hyper-geometric distribution would be more appropriate.

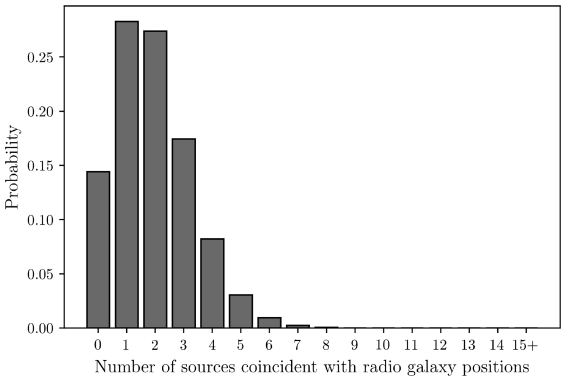

Figure 2. The probability distribution that characterizes the probability of y number of chance correlations of spatially coincident sub-threshold γ-ray excesses with the positions of TRGs in our sample. The bins of $y = 15$–72 are combined, due to their very low probability.

5.2 Sample galaxy core dominance

The core dominance is a general measure of the intensity of the radio flux at the core of a galaxy with respect to the total radio emission of the galaxy. Giovannini et al. (1994) suggest that measured core dominance of a galaxy could provide a measure of the orientation angle of jet, with a more dominant radio core indicating a smaller orientation angle. In blazars we are looking directly down the jet, and thus there is strong core dominance in this class of AGNs. As γ-rays in blazars are intensified by Doppler boosting in the jets, if kpc-scale jet emission in fact dominates the 4FGL galaxies in our sample (rather than large-scale processes) the detected galaxies will tend towards the higher end of the core dominance distribution.

We take the core dominance values from the VLA observations of the BCS quoted in Liuzzo et al. (2009) as these provide an almost complete representation of the radio galaxies in the BCS, although there are other ways of defining and calculating the core dominance, such as Fan & Zhang (2003). The values from Liuzzo et al. (2009) correspond to the ratio between observed and estimated core radio power (Giovannini et al. 1994), with a value greater than 1 indicating a Doppler-boosted core, and less than 1 indicating a deboosted core. VLA observations of the BCS are incomplete, but data are available for 57 galaxies in the sample (including all six 4FGL radio galaxies and two STRGs: 3C 272.1 and B2 1040+31). For a further five galaxies in our sample, there are upper limits to core dominance available; one of these is the STRG 3C 293. Fig. B3 shows the distribution of core dominances for each radio galaxy.

Considering the 4FGL radio galaxies in the sample, 3C 264 has a core dominance value of just above 1, indicating mild boosting. NGC 2484, 4C 39.12, and NGC 315 all have core dominance values greater than 3, indicating stronger Doppler boosting in the core. This is indicative of strongly jet-dominated γ-ray emission. The exceptional 4FGL radio galaxy is 3C 274 (M 87), where a core dominance of <1 indicates a deboosted core.

For the STRGs where we have values for core dominance, these are generally smaller than those of the 4FGL galaxies, with none of them above 1, although the sample size is small. Both 4C 29.41 and 3C 272.1 have core dominance values below 1, indicating that any emission from these radio galaxies may not originate from processes in the kpc-scale jet, similar to the emission causing the spectral component seen in the core of Cen A, as discussed in Brown et al. (2017), and searched for in Rulten et al. (2020) (for example, emission from a parsec-scale inner jet, or an additional population of cosmic rays). In the case of 3C 293, a 95 per cent confidence limit is in place of a measurement with a maximum value of 1.42. Thus, it is difficult to conclude whether this radio galaxy is Doppler boosted or not.

The majority of our overall sample is boosted, with core dominance values greater than 1. This includes most of the γ-ray-emitting 4FGL radio galaxies. The STRGs for which we have data are not generally among these, with only 3C 293 possibly being mildly boosted.

6 DISCUSSION

One motivating factor in choosing the BCS as the basis for our survey is that the redshifts and optical magnitudes of its radio galaxies are consistent with those of the 4FGL radio galaxies. Within this distribution, the STRGs are neither particularly bright nor close, so it is difficult to understand why we might see γ-ray emission from these four radio galaxies in particular. This reinforces the conclusion in Section 5, which suggests that the γ-ray emission is likely just a chance association.

The core dominance values described in Section 5 indicate that the 4FGL radio galaxies have Doppler-boosted jet dominant emission, which prevents us from observing any non-jet emission, should it be present. The only 4FGL radio galaxy in the BCS that is not core dominant is 3C 274, better known as M 87 (Beilicke et al. 2007; Abdo et al. 2009). M 87 is a unique case, as it is a very massive galaxy at the centre of the Virgo supercluster and like Cen A it is close to the Earth ($z = 0.0043$). As a deboosted radio galaxy, it is likely that some of the observed γ-ray emission occurs close to the black hole (Acciari et al. 2009) and not in the kpc jet, a hypothesis backed up by M 87's variable nature. However, as the core and jet cannot be resolved from one another in γ-rays (unlike Cen A), it is more difficult to distinguish between jet and core emission. Furthermore, the spectral shape in M 87 is variable and this makes it exceptionally difficult to identify persistent spectral features like the hardening observed in Cen A (which is non-variable on the time-scale of the *Fermi*-LAT mission, with a variability index of 8.25 in the 4FGL).

Comparing the core dominance values of the STRGs and the 4FGL radio galaxies, we find that (with the exception of 3C 274/M 87) these are not consistent with one another, as the 4FGL radio galaxies appear to have kpc-jet-dominated emission, while the STRGs do not. Given that the STRGs are neither particularly bright nor particularly close, this further reinforces the conclusion that this apparent γ-ray emission is likely a chance association.

Angioni et al. (2019) find a correlation between radio core flux density and observed γ-ray luminosity in a sample of radio galaxies. However, they also find other indicators suggesting that the observed γ-ray emission is not due to Doppler boosting in the kpc jets (such as a lack of correlation between γ-ray luminosity and core dominance), providing evidence for γ-ray emission that is not from the kpc-scale jet. Fig. B4 displays γ-ray flux plotted against core dominance; this is consistent with Angioni et al. (2019) and Rulten et al. (2020), who find no correlation between γ-ray luminosity and core dominance in their analysis of the known 4FGL radio galaxies. Although these authors use a different method to calculate core dominance to Liuzzo et al. (2009), which we use, all use radio measurements at similar frequencies (5 and 8.4 GHz, respectively). This supports the hypothesis that observable γ-ray

emission is not necessarily linked to core dominance at these radio frequencies.

Assuming that the photon counts of the four STRGs grow linearly with time, we can estimate how much more *Fermi*-LAT observations we would require for these objects to reach the 5σ level. For the most significant of our four STRGs, B2 0800+24, this is 6 yr. None the less, given the potentially variable nature of radio galaxies, it is worth monitoring the STRGs for changes in source significance and γ-ray flux.

7 CONCLUSIONS

We executed an unbiased survey of radio galaxies with *Fermi*-LAT targeting radio galaxies from the BCS, with the hypothesis that any detectable γ-ray emission could be caused by mechanisms other than the jet. We find some γ-ray emission spatially coincident with four of these, but there is insufficient evidence to claim a detection. Furthermore, a calculation to understand the impact of the look-elsewhere effect on our survey suggests that this γ-ray emission is likely to be a chance correlation. This is supported by the fact that these four STRGs are generally unremarkable, giving no explanation as to why these four in particular might be observed out of the entire sample. We calculate flux limits for all of the TRGs and STRGs radio galaxies in our sample.

The question of whether any γ-ray emission can be detected from non-jet processes in AGNs therefore remains an open one. However, given the dominance of radio galaxies in the AGN population, further studies, using different catalogues and selection criteria, are warranted.

ACKNOWLEDGEMENTS

The authors would like to acknowledge the excellent data and analysis tools provided by the NASA *Fermi* collaboration, without which this work could not be done. In addition, this research has made use of the NASA/IPAC Extragalactic Database (NED) that is operated by the Jet Propulsion Laboratory, California Institute of Technology, under contract with the National Aeronautics and Space Administration, and the SIMBAD data base, operated at CDS, Strasbourg, France and Montage, funded by the National Science Foundation. We would also like to thank Matthew Capewell, Alastair Edge, Jamie Graham, and Anthony Brown for useful discussions, and the referee for valuable feedback on this work.

MH acknowledges funding from Science and Technology Facilities Council (STFC) PhD Studentship ST/S505365/1, and PMC and CBR acknowledge funding from STFC consolidated grant ST/P000541/1.

REFERENCES

Abdo A. A. et al., 2009, ApJ, 707, 55
Abdo A. et al., 2010, Science, 328, 725
Abdollahi S. et al., 2020, ApJS, 247, 33
Acciari V. A. et al., 2009, Science, 325, 444
Ackermann M. et al., 2016, ApJ, 826, 1
Angioni R. et al., 2019, A&A, 627, A148
Atwood W. B. et al., 2009, ApJ, 697, 1071
Baldi R. D., Capetti A., 2009, A&A, 508, 603
Baldi R. D., Capetti A., Giovannini G., 2016, Astron. Nachr., 337, 114
Beilicke M., et al., 2007, AIP Conference Proceedings, 921, 147
Bennett A. S., 1962, MNRAS, 125, 75
Boettcher M., Reimer A., Sweeney K., Prakash A., 2013, ApJ, 768, 54
Brown A. M., Boehm C., Graham J., Lacroix T., Chadwick P., Silk J., 2017, Phys. Rev. D, 95, 063018
Colla G. et al., 1970, A&AS, 1, 281
Colla G. et al., 1972, A&AS, 7, 1
Colla G. et al., 1973, A&AS, 11, 291
Fan J. H., Zhang J. S., 2003, A&A, 407, 899
Fanaroff B. L., Riley J. M., 1974, MNRAS, 167, 31 P
Fanti C., Fanti R., Ficarra A., Padrielli L., 1974, A&AS, 18, 147
Garofalo D., Singh C. B., 2019, ApJ, 871, 259
Giovannini G., Feretti L., Comoretto G., 1990, ApJ, 358, 159
Giovannini G., Feretti L., Venturi T., Lara L., Marcaide J., Rioja M., Spangler S. R., Wehrle A. E., 1994, ApJ, 435, 116
Giovannini G., Taylor G. B., Feretti L., Cotton W. D., Lara L., Venturi T., 2005, ApJ, 618, 635
Grandi P., Torresi E., 2012, Fermi and Jansky Proceedings - eConf C1111101
Janiak M., Sikora M., Moderski R., 2016, MNRAS, 458, 2360
Kataoka J. et al., 2010, ApJ, 715, 554
Liuzzo E., Giovannini G., Giroletti M., Taylor G. B., 2009, A&A, 505, 509
Lyons L., 2008, Ann. Appl. Stat., 2, 887
Massaro F., Thompson D. J., Ferrara E. C., 2016, A&AR, 24, 2
Mattox J. R. et al., 1996, ApJ, 461, 396
Owen F. N., Ledlow M. J., 1994, Phys. Act. Galaxies, 54, 319
Rulten C. B., Brown A. M., Chadwick P. M., 2020, MNRAS, 492, 4666
Sanchez D. et al., 2018, Proceedings of the TeVPA Conference
Tanada K., Kataoka J., Arimoto M., Akita M., Cheung C. C., Digel S. W., Fukazawa Y., 2018, ApJ, 860, 74
Urry C. M., Padovani P., 1995, PASP, 107, 803
Wilks S. S., 1938, Ann. Math. Stat., 9, 60
Wood M., Caputo R., Charles E., Di Mauro M., Magill J., Perkins J., 2017, PoS, ICRC2017, 824,

APPENDIX A: RADIO GALAXY SAMPLE

Table A1. The radio galaxies selected from the BCS for use as targets in our search with the *Fermi*-LAT data. The galaxy redshifts are from Giovannini et al. (2005), and the RA and Dec values are taken from the NASA/IPAC Extragalactic Database (NED), and quoted where appropriate to two decimal places. $E^2\frac{\mathrm{d}N}{\mathrm{d}E}$ is the energy multiplied by the differential flux for a bin of an SED, with units of $\mathrm{MeVcm^{-2}s^{-1}}$. To obtain the flux limits quoted, we calculate a single bin SED across our entire analysed energy range at the position of each TRG where no source is detected. Where a source is detected (in the case of the STRGs and 4FGL sources), we compute our upper limit for this source instead.

Galaxy name	Morphology	Redshift	RA (°)	Dec (°)	Flux limit	γ-rays detected?
4C 39.12	FR 0	0.0202	53.58	39.36	2.78×10^{-6}	Yes, in 4FGL
4C 31.04	FR 0	0.0592	19.9	32.18	6.00×10^{-8}	No
B2 0222+36	FR 0	0.0327	36.36	37.17	8.08×10^{-8}	No
B2 0648+27	FR 0	0.0409	53.58	27.46	8.35×10^{-8}	No
4C 30.19	FR 0	0.0909	160.13	29.97	2.83×10^{-8}	No
B2 1040+31	FR 0	0.036	160.83	31.52	8.77×10^{-7}	STRG

Table A1 – *continued*

Galaxy name	Morphology	Redshift	RA (°)	Dec (°)	Flux limit	γ-rays detected?
N4278	FR 0	0.0021	185.03	29.28	4.76×10^{-8}	No
B2 1512+30	FR 0	0.0931	228.52	30.15	1.39×10^{-8}	No
IC 4587	FR 0	0.0442	239.97	25.94	2.76×10^{-8}	No
B2 1855+37	FR 0	0.0552	284.41	38.01	2.78×10^{-8}	No
UGC 367	FR I	0.0321	9.27	25.7	5.69×10^{-8}	No
NGC 326	FR I	0.0472	14.6	26.87	1.17×10^{-8}	No
NGC 315	FR I	0.0167	14.45	30.35	2.64×10^{-6}	Yes, in 4FGL
3C 31	FR I	0.0169	16.85	32.41	8.41×10^{-8}	No
NGC 507	FR I	0.0164	20.92	33.26	2.08×10^{-8}	No
NGC 708	FR I	0.016	28.19	36.15	4.53×10^{-8}	No
4C 35.03	FR I	0.0375	32.41	35.8	2.41×10^{-8}	No
3C 66B	FR I	0.0215	35.8	42.99	2.15×10^{-7}	No
3C 76.1	FR I	0.0328	45.81	16.44	3.09×10^{-8}	No
B2 0326+39	FR I	0.0243	52.35	39.8	1.75×10^{-8}	No
B2 0708+32	FR I	0.0672	107.94	32.05	1.74×10^{-8}	No
NGC 2484	FR I	0.0413	119.6	37.78	1.29×10^{-6}	Yes, in 4FGL
B2 0800+24	FR I	0.0433	120.82	24.68	1.33×10^{-6}	STRG
4C 32.26	FR I	0.068	130.3	32.42	2.07×10^{-8}	No
B2 0913+38	FR I	0.0711	139.17	38.68	9.79×10^{-8}	No
B2 0915+32	FR I	0.062	139.53	32.43	2.60×10^{-8}	No
B2 1102+30	FR I	0.072	166.35	30.16	4.27×10^{-8}	No
4C 29.41	FR I	0.0489	169.1	29.25	1.25×10^{-6}	Yes, 4FGL
B2 1116+28	FR I	0.0667	169.75	27.9	2.08×10^{-8}	No
NGC 3665	FR I	0.0067	171.18	38.76	5.91×10^{-8}	No
3C 264	FR I	0.0206	176.27	19.61	3.03×10^{-6}	Yes, in 4FGL
B2 1144+35	FR I	0.063	176.71	35.48	1.39×10^{-8}	No
B2 1204+24	FR I	0.0769	181.78	23.91	4.45×10^{-8}	No
3C 272.1	FR I	0.0037	186.27	12.89	1.04×10^{-6}	STRG
3C 274 (M 87)	FR I	0.0043	187.71	12.39	1.31×10^{-5}	Yes, in 4FGL
B2 1243+26B	FR I	0.0891	191.58	26.45	2.00×10^{-8}	No
NGC 4839	FR I	0.0246	194.35	27.5	5.58×10^{-8}	No
NGC 4869	FR I	0.0224	194.85	27.91	3.99×10^{-8}	No
NGC 4874	FR I	0.0239	194.9	27.96	4.31×10^{-8}	No
4C 29.47	FR I	0.0728	199.77	29.64	1.53×10^{-8}	No
NGC 5127	FR I	0.0161	200.94	31.57	5.53×10^{-8}	No
NGC 5141	FR I	0.0175	201.21	36.38	3.06×10^{-8}	No
B2 1339+26	FR I	0.0722	205.46	26.37	6.22×10^{-8}	No
4C 26.42	FR I	0.0633	207.29	26.59	3.77×10^{-8}	No
3C 293	FR I	0.0452	208.07	31.45	8.80×10^{-7}	STRG
B2 1357+28	FR I	0.0629	210.0	28.5	1.60×10^{-8}	No
3C 296	FR I	0.0237	214.22	10.81	8.41×10^{-8}	No
4C 25.46	FR I	0.0813	218.18	24.93	3.30×10^{-8}	No
B2 1441+26	FR I	0.0621	221.03	26.02	9.04×10^{-9}	No
3C 305	FR I	0.041	222.34	63.27	4.06×10^{-8}	No
3C 310	FR I	0.054	226.24	26.02	6.28×10^{-8}	No
B2 1525+29	FR I	0.0653	231.94	28.92	1.92×10^{-8}	No
B2 1528+29	FR I	0.0843	232.54	29.01	3.20×10^{-8}	No
NGC 6086	FR I	0.0313	243.15	29.49	5.15×10^{-8}	No
B2 1613+27	FR I	0.0647	243.88	27.5	4.93×10^{-8}	No
NGC 6107	FR I	0.0296	244.33	34.9	3.49×10^{-8}	No
NGC 6137	FR I	0.031	245.76	37.92	1.79×10^{-8}	No
3C 338	FR I	0.0303	247.16	39.55	3.71×10^{-8}	No
B2 1637+29	FR I	0.0875	249.83	29.85	3.28×10^{-8}	No
4C 32.52	FR I	0.0631	254.75	32.49	6.02×10^{-8}	No
4C 30.31	FR I	0.0351	255.19	30.14	4.97×10^{-8}	No
B2 1736+32	FR I	0.0741	264.65	32.93	1.13×10^{-8}	No
B2 1752+32B	FR I	0.0449	268.65	32.57	3.79×10^{-8}	No
3C 449	FR I	0.0181	337.84	39.36	3.47×10^{-8}	No
B2 2236+35	FR I	0.0277	339.62	35.33	3.72×10^{-8}	No
3C 465	FR I	0.0301	354.62	27.03	5.98×10^{-8}	No
3C 33	FR II	0.0595	17.21	13.31	1.83×10^{-8}	No
3C 98	FR II	0.0306	59.73	10.43	2.18×10^{-8}	No
3C 192	FR II	0.0597	121.36	24.16	3.04×10^{-8}	No
4C 32.15	FR II	0.0507	60.08	32.51	9.86×10^{-8}	No

Table A1 – *continued*

Galaxy name	Morphology	Redshift	RA (°)	Dec (°)	Flux limit	γ-rays detected?
IC 2402	FR II	0.0675	132.0	31.79	3.39×10^{-8}	No
3C 236	FR II	0.0989	151.51	34.9	1.69×10^{-8}	No
3C 277.3	FR II	0.0857	193.4	27.1	4.74×10^{-8}	No
3C 321	FR II	0.096	232.93	24.07	3.21×10^{-8}	No
3C 326	FR II	0.0895	238.04	20.09	4.07×10^{-8}	No
3C 382	FR II	0.0586	278.76	32.7	5.01×10^{-8}	No
3C 388	FR II	0.0917	281.01	45.56	1.42×10^{-8}	No
3C 390.3	FR II	0.0569	280.54	79.77	6.78×10^{-7}	No

APPENDIX B: ADDITIONAL FIGURES

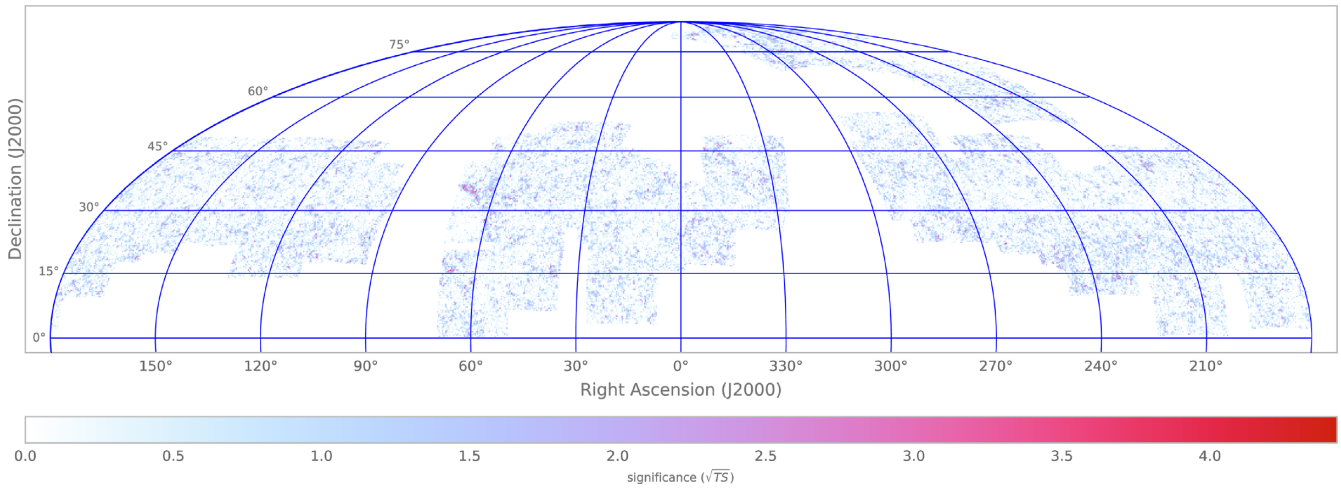

Figure B1. A TS map of all the analysed ROIs across the Northern hemisphere. Coloured regions indicate where observations and modelling have taken place, white regions have not been analysed. The colour scale shows the significance (square root of TS) of each bin, and largely shows random fluctuations from the Galactic and isotropic γ-ray diffuse backgrounds. As this map was generated *after* the 'find sources' algorithm, the upper limit on TS is approximately 16, as almost all of the points with a higher TS than this have been fitted with a point source. This map shows no significant areas of γ-ray excess that are not fitted by a model, so we can be confident that our modelling was successful.

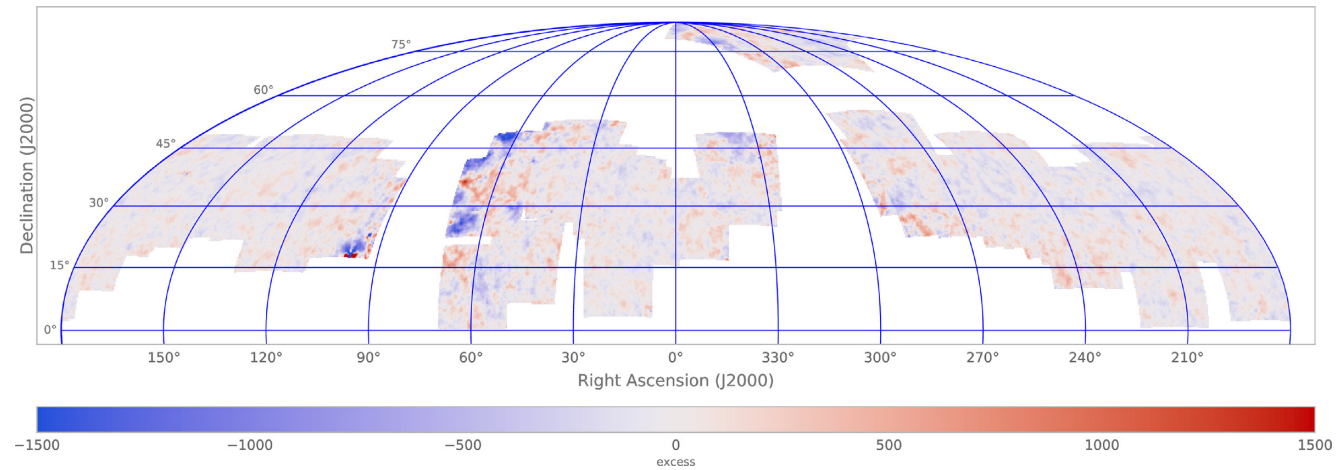

Figure B2. The residual map of all of the analysed ROIs, across the Northern hemisphere. Coloured regions indicate where observations and modelling have taken place; white regions show where there are no data. The colour scale shows residual counts, and consistently averages to around 0. The areas of poorer quality modelling adjacent to the left- and right-hand vertical white areas are due to edge effects from the Galactic plane. This plot also shows that the ROIs overlap with one another, necessitating that we treat the TRGs independently.

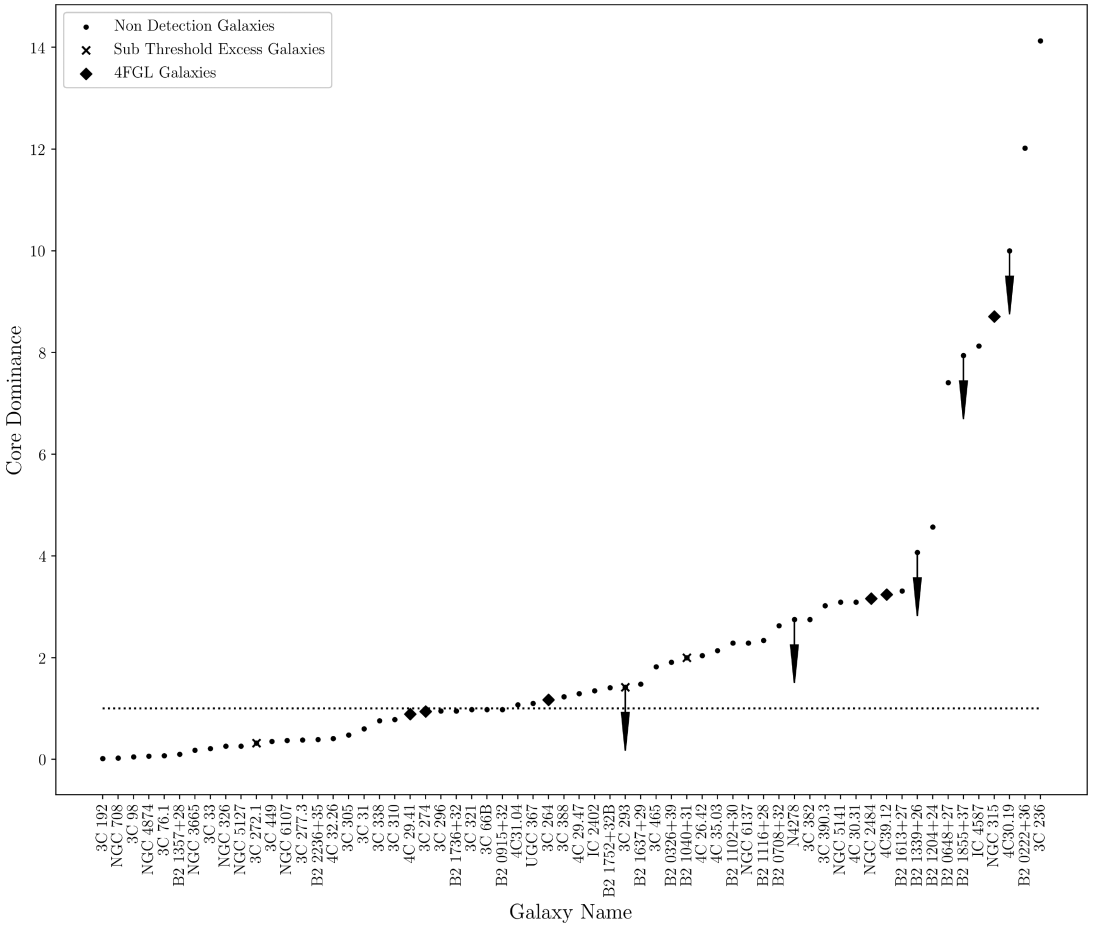

Figure B3. The distribution of the known core dominance values for the radio galaxies in the BCS, using values from Liuzzo et al. (2009). Not all of the radio galaxies in our sample have measurements of core dominance, and thus we cannot show a value for every TRG in the sample. Downward facing arrows indicate a 95 per cent confidence limit, rather than an accurate measure of core dominance. The grey dashed line indicates a core dominance of 1. Radio galaxies above this line are therefore Doppler boosted in their jets, and those below are deboosted. Known 4FGL radio galaxies are indicated by a diamond and the STRGs with a cross.

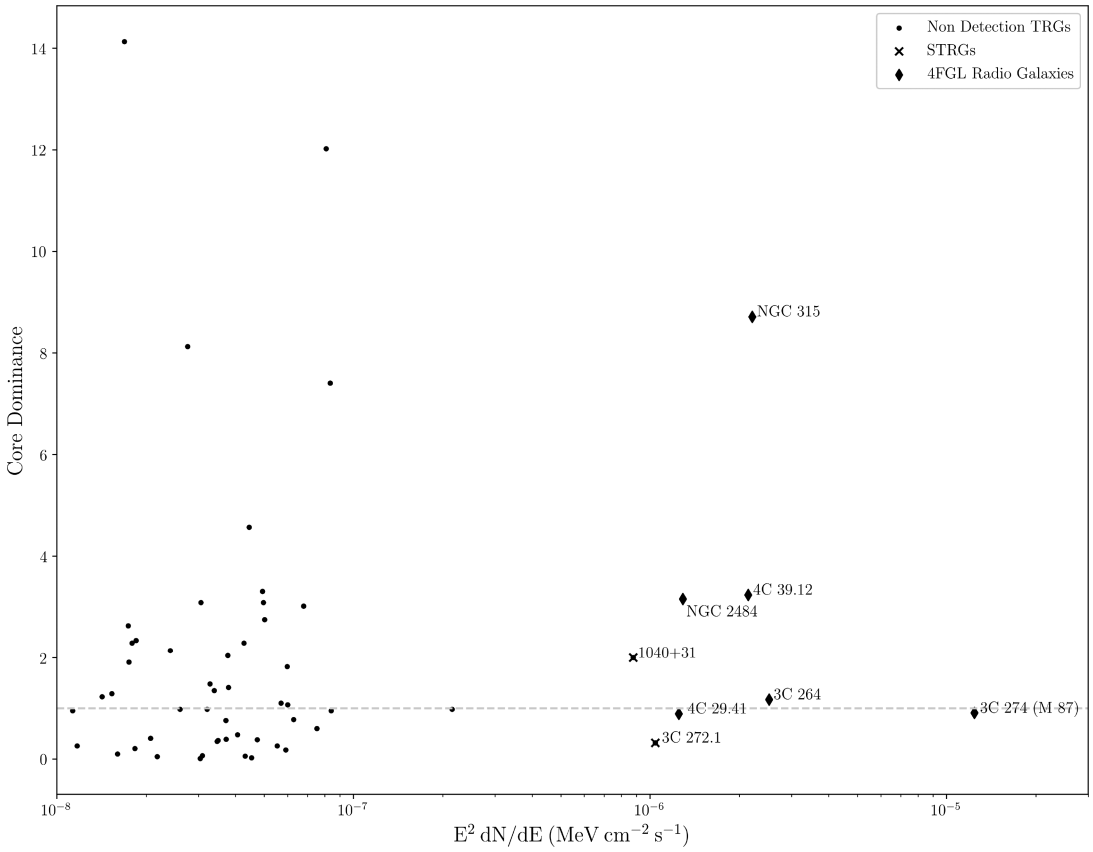

Figure B4. The distribution of known core dominance values for the radio galaxies in the BCS, plotted against the calculated γ-ray flux values shown in Table A1. All values are upper limits, except the significant detections 4C 39.12, NGC 315, 3C 264, and 3C 274 (M 87) where the actual flux values are used. The grey dashed line indicates a core dominance of 1. Radio galaxies above this line are therefore Doppler boosted in their jets, and those below are deboosted. Known 4FGL radio galaxies are indicated by a diamond and the STRGs with a cross, and are labelled.

This paper has been typeset from a TEX/LATEX file prepared by the author.